MALAYSIAN JOURNAL OF SCIENCE
MJS
ISSN 1394-3065

Regular Issue

Malaysian Journal of Science 44 (2): 52-62 (June 2025) https://mjs.um.edu.my

Bogdanov-Takens Bifurcation in SIRI Model with Multiple Reinfection of COVID-19

Livia Owen[1]

Abstract: In the presence of cases of COVID-19 reinfection, we propose a SIRI (Susceptible-Infected-Recovery-Infected) spread model of two COVID-19 variants. This model considers the possibility of individuals becoming reinfected with the same or different variants, although the risk of reinfection with the same variant remains lower due to natural immunity from previous infections. Besides analyzing the stability of equilibrium points, we focus on codimension-one bifurcations. Our initial numerical simulations used parameters obtained from real data collected through a British government survey. Our analysis revealed unstable disease-free equilibria and stable endemic equilibria. By varying the Case Fatality Rate parameter, we identified all codimension-one bifurcations. To further investigate the model's dynamics, we introduced a new parameter, the reinfection rate, and utilized AUTO software. Our research led to the discovery of codimension-two bifurcations, specifically the Bogdanov-Takens bifurcation. We identified the parameter domain where a stable limit cycle and homoclinic orbit occur in the presence of the Bogdanov-Takens bifurcation. We also simulated parameter variations that could trigger a pandemic resurgence. This highlights the possibility of emerging variants causing a pandemic return.

Keywords: *SIRI, reinfection, COVID-19, codimension one bifurcation, Bogdanov-Takens bifurcation.*

1. Introduction

Since December 2019, the Coronavirus Disease 2019, commonly known as COVID-19, has been spreading and affecting the world. The origin of COVID-19 is believed to be in a seafood market in Wuhan, China. The World Health Organization (WHO) declared COVID-19 a pandemic on March 11, 2020, and there have been over 770 million reported cases of COVID-19, resulting in over 6.9 million deaths (WHO, 2023). Recently, in August 2023, there were reports of over 1.4 million new COVID-19 cases and 1,800 fatalities. The four major variants of COVID-19 are Alpha, Beta, Delta, and Omicron. Omicron has subvariants such as XBB and Eris, which are still considered "Variants of Interest" because of their high transmission potential. The WHO designates these variants as VOI to monitor their spread. A new highly mutated variant named Pirola has been detected in the UK (Yale, 2023).

During the Omicron wave, there have been instances of reinfection with the same or different variants. Individuals can contract COVID-19 multiple times (Pinto et al., 2021; WHO, 2023). COVID-19 sequences by variant and subvariant of Omicron in each country can be viewed on (Our World in Data, 2023). On average, there are two predominant variants of the epidemic during a given interval, as shown in Figure 1. For example, as of April 12, 2021, the two prevalent varieties were the Alpha and Beta variants. One month later, the two prevalent varieties were the Alpha and Delta variants. On December 20, 2021, the two dominant variants were the Delta and Omicron (BA.1) variants. Currently, two subvariants of Omicron are predominant.

Authors information:
[a]Center for Mathematics and Society, Department of Mathematics, Parahyangan Catholic University, Bandung 40141, INDONESIA. E-mail: livia.owen@unpar.ac.id[1];
*Corresponding Author: livia.owen@unpar.ac.id

Received: June 8, 2023
Accepted: June 20, 2024
Published: June 30, 2025

DOI:https//doi.org/10.22452/mjs.vol44no2.5
Malaysian Journal of Science 44(2): 52-62 (June 2025)

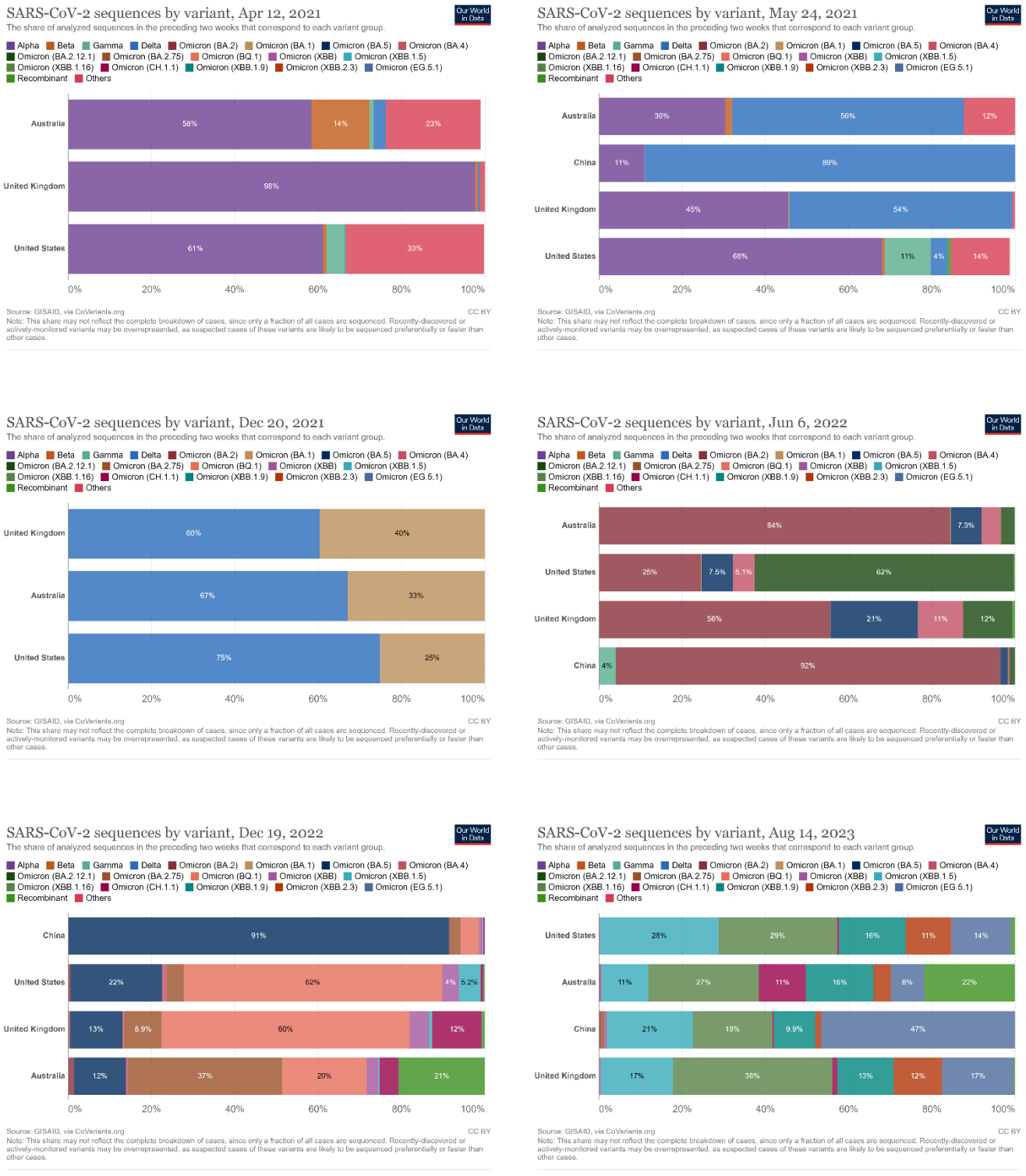

Figure 1. COVID-19 sequences by variant from June 7 in Australia, China, UK, United States, June 7, 2021 until April 26, 2023 (Our World in Data, 2023).

DOI:https//doi.org/10.22452/mjs.vol44no2.5
Malaysian Journal of Science 44(2): 52-62 (June 2025)

The complexity of COVID-19's spread is compounded by the possibility of reinfection with the same or different virus variants. To gain deeper insight into disease spread under these circumstances, we propose a SIRI (Susceptible-Infected-Recovery-Infected) model for two COVID-19 variants. Previous SIRI spread model research appears in studies on TBC and herpes disease spread models (Sharma et al., 2017), SIRI diffusion models (Yang, 2019; Duan, 2021), and vaccination strategies (Martins & Pinto, 2017). Recent SIRI model research on COVID-19 spread is detailed in (Nurjanah, 2022), while the discrete model appears in (McMahon & Robb, 2020). Studies by (Wangari, 2021) and (Salman, 2021) examined COVID-19 reinfection using data from Kenya and Malaysia, respectively. Reinfection in COVID-19 significantly impacts modeling processes. However, these studies considered only one disease variant and have not addressed multi-strain disease spread models. Our paper examines how public awareness affects COVID-19 spread, considering same-strain reinfection possibilities. The study analyzes the virus's multi-strain spread model, helping policymakers and healthcare professionals understand public awareness's role in reducing COVID-19 transmission.

This research develops from studies examining COVID-19 spread models with saturation. A discrete version appears in (Yong et al., 2022a), and proposed government policy design appears in (Yong et al., 2022b). Codimension 1 bifurcation analysis and interpretation appear in (Yong et al., 2022a). The study uses public awareness level as its bifurcation parameter. From basic reproduction numbers, we analyze disease-free equilibria point stability. We derive endemic equilibrium points and analyze their bifurcations. The first numerical simulation uses parameters from British government survey data (ONS, 2023) in Table 1. These data indicate that recovered individuals cannot experience reinfection from previous variants. Consequently, our model assumes reinfection occurs only with the same variant or new variants. Beyond real-data parameters, we simulate parameter variations that could trigger pandemic resurgence, representing potential scenarios if new variants emerge.

Table 1. Percentage of first and second infections by period in which different variants were dominant, UK, 2 July 2020 to 23 November 2022 (ONS, 2023)

First infection variant	Second infection variant	Estimated percentage (%) of total reinfection
Alpha	Alpha	1.1
Alpha	Delta	4.4
Alpha	Omicron BA.1	9.9
Alpha	Omicron BA.2	10.6
Alpha	Omicron BA.4/BA.5	9.5
Delta	Delta	0.6
Delta	Omicron BA.1	8.2
Delta	Omicron BA.2	11.5
Delta	Omicron BA.4/BA.5	12.9
Omicron BA.1	Omicron BA.1	0.3
Omicron BA.1	Omicron BA.2	4.9
Omicron BA.1	Omicron BA.4/BA.5	16.6
Omicron BA.2	Omicron BA.2	0.3
Omicron BA.2	Omicron BA.4/BA.5	8.5
Omicron BA.4/BA.5	Omicron BA.4/BA.5	0.7

2. Model

After the recent case of reinfection, we modified the SIRS model to use the SIRI model due to the multi-strain variant we work with. This model allows individuals with recovery to become infected with the same or a different variant. We constructed our model based on the following assumptions, see Figure 2.

We denoted two main variants of COVID-19, i.e., $i = 1$ for the past variant and $i = 2$ for the new or current variant (including all of the subvariants). Let $S = S(t)$, $I_i = I_i(t)$, and $R_i = R_i(t)$ respectively, the number of susceptible individuals, infected by i-variant individuals, and recovered individuals at time $t \geq 0$.

We excluded the exposed individual because, according to the European Centre for Disease Prevention and Control, the incubation time for the new variant is shorter (3-4 days).

The recruitment of individuals due to births and migrations is constant, Λ and also proportional to the number of recovery individuals: $\lambda(R_1 + R_2)$ for Λ, $\lambda > 0$, and they assumed as susceptible individuals.

The incidence rate is proportional to the possible contacts between susceptible individuals and infected individuals and has a denominator which increases with S. The parameter γ_1 measuring the level of a susceptible's cautiousness. So we have the incidence rate: $\frac{\beta_i S I_i}{1+\gamma_1 S}$ for some $\beta_i > 0$.

Infected individuals I_i become recovered R_i at the rate $\mu_i > 0$.

The proportions of each individual leaving the population as a result of deaths are proportional to the mortality rate $\delta > 0$. Infected individuals die at a greater rate than susceptible and recovered individuals, so we add the Case Fatality Rate (CFR) of each variant, δ_i.

Recovery individuals R_1 can be reinfected with the same variant with rate α_{11} or by new variant with rate α_{12}. Recovery individuals

DOI:https//doi.org/10.22452/mjs.vol44no2.5
Malaysian Journal of Science 44(2): 52-62 (June 2025)

R_2 only reinfected with the same variant with rate α_{22} and cannot be reinfected by the old variant, see Table 1. This incidence rate is proportional to the possible contacts of recovery and infected individuals and also the reinfection rate from i variant to j variant, $i, j = 1, 2$. The level of recovery's cautiousness is assumed to be less than or equal to the level of susceptible's one, $\gamma_2 \leq \gamma_1$, thus we have the incidence rate: $\frac{\alpha_{ij}\beta_i R_i I_j}{1+\gamma_2 R_i}$ for some $i, j = 1,2, i \leq j$.

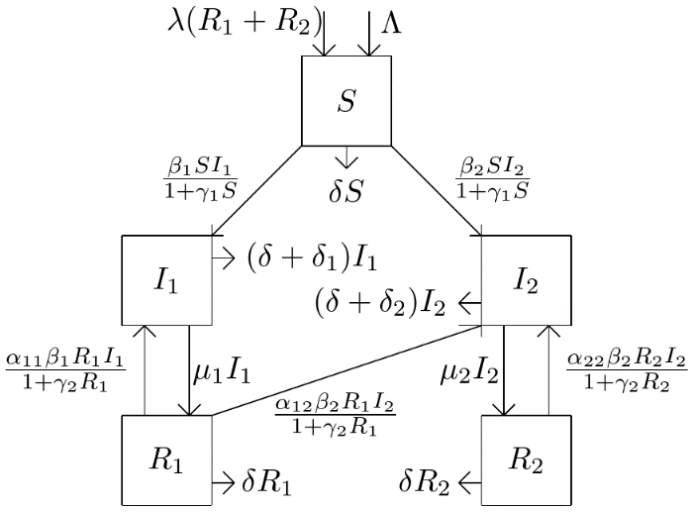

Figure 2. Transmission diagram of COVID-19

Table 2. The model parameters with their biological meanings

Parameters	Biological meanings	Estimated values	Sources
α_{ij}	Reinfection rate from i to j variant, $i \leq j$,	(0.01,0.35)	(ONS, 2023)
β_i	Transmission coefficient from susceptible to infected individuals with i variant.	(0.58,0.95)	(Ndairou et al., 2020)
δ	Mortality rate	0.002	(Ud Din et al., 2020)
δ_i	Case Fatality Rate (CFR) i variant	(0.01,0.05)	(Ndairou et al., 2020)
Λ	Recruitment of susceptible individuals (birth rate, etc.)	$\frac{10000}{59 \times 365}$	(Agusto, 2013)
λ	Birth rate of recovery individual	(0.01, 0.2)	(Ud Din et al., 2020)
μ_i	Recovery rate of i variant	(0.5, 0,8)	(Ndairou et al., 2020)
γ_1	The susceptible individual's cautiousness level	(0.3,0.8)	(Yong et al., 2022b)
γ_2	The recovery individual's cautiousness level, $\gamma_2 < \gamma_1$	(0.3,0.8)	(Yong et al., 2022b)

The above assumptions lead to the following model:

$$\begin{cases} \frac{dS}{dt} &= \Lambda + \lambda(R_1 + R_2) - \delta S - \frac{\beta_1 SI_1}{1+\gamma_1 S} - \frac{\beta_2 SI_2}{1+\gamma_1 S}, \\ \frac{dI_1}{dt} &= \frac{\beta_1 SI_1}{1+\gamma_1 S} - \delta I_1 - \delta_1 I_1 - \mu_1 I_1 + \frac{\alpha_{11}\beta_1 I_1 R_1}{1+\gamma_2 R_1}, \\ \frac{dI_2}{dt} &= \frac{\beta_2 SI_2}{1+\gamma_1 S} - \delta I_2 - \delta_2 I_2 - \mu_2 I_2 + \frac{\alpha_{22}\beta_2 I_2 R_2}{1+\gamma_2 R_2} + \frac{\alpha_{12}\beta_2 I_2 R_1}{1+\gamma_2 R_1}, \\ \frac{dR_1}{dt} &= \mu_1 I_1 - \delta R_1 - \frac{\alpha_{11}\beta_1 I_1 R_1}{1+\gamma_2 R_1} - \frac{\alpha_{12}\beta_2 I_2 R_1}{1+\gamma_2 R_1}, \\ \frac{dR_2}{dt} &= \mu_2 I_2 - \delta R_2 - \frac{\alpha_{22}\beta_2 I_2 R_2}{1+\gamma_2 R_2}, \end{cases} \quad (1)$$

DOI:https//doi.org/10.22452/mjs.vol44no2.5
Malaysian Journal of Science 44(2): 52-62 (June 2025)

3. Results and Discussion

Firstly, we applied the following proposition regarding the System's positiveness solution.

Proposition 1. (The System's positiveness solution.) Let the initial conditions: $S(0), I_i(0), R_i(0) \geq 0, i, j = 1,2$, then the solutions $S(t), I_i(t), R_i(t), i, j = 1,2$ of system (1) are non- negative for $t \geq 0$.

Proof 1. Rewrite the right hand side of $\frac{dI_1}{dt}$ and $\frac{dI_2}{dt}$ on System (1) as

$$\begin{aligned} \frac{dI_1}{dt} &= I_1\left(\frac{\beta_1 S}{1+\gamma_1 S} - \delta - \delta_1 - \mu_1 + \frac{\alpha_{11}\beta_1 R_1}{1+\gamma_2 R_1}\right), \\ \frac{dI_2}{dt} &= I_2\left(\frac{\beta_2 S}{1+\gamma_1 S} - \delta - \delta_2 - \mu_2 + \frac{\alpha_{22}\beta_2 R_2}{1+\gamma_2 R_2} + \frac{\alpha_{12}\beta_2 R_1}{1+\gamma_2 R_1}\right). \end{aligned}$$

Both planes $I_1 = 0$ and $I_2 = 0$ are invariant manifolds since it imply $\frac{dI_1}{dt} = 0$ and $\frac{dI_2}{dt} = 0$.

Since $\frac{dS}{dt}\Big|_{S=0,I_1,I_2,R_1,R_2\geq 0} = \Lambda + \lambda(R_1 + R_2), \frac{dR_1}{dt}\Big|_{R_1=0,S,I_1,I_2,R_2\geq 0} = \mu_1 I_1, \frac{dR_2}{dt}\Big|_{R_2=0,S,I_1,I_2,R_1\geq 0} = \mu_2 I_2$, the rates listed above are all non-negative over their $\mathbb{R}^5_+$ boundary planes. As a result, we have the vector fields intended inward direction from their boundaries. Starting with non-negative initial conditions so that all of the System's solutions (1) remain positive for all $t \geq 0$. ■

The Basic Reproduction Number and The Stability of the Disease-Free Equilibrium

The disease-free equilibrium is $E_0 = \left(\frac{\Lambda}{\delta}, 0,0,0,0\right)$ and the linearized vector field of (1) in the vicinity of E_0 is

$$\begin{pmatrix} -\delta & -\frac{\beta_1\Lambda}{\gamma_1\Lambda+\delta} & -\frac{\beta_2\Lambda}{\gamma_1\Lambda+\delta} & \lambda & \lambda \\ 0 & -\delta-\delta_1-\mu_1+\frac{\beta_1\Lambda}{\gamma_1\Lambda+\delta} & 0 & 0 & 0 \\ 0 & 0 & -\delta-\delta_2-\mu_2+\frac{\beta_2\Lambda}{\gamma_1\Lambda+\delta} & 0 & 0 \\ 0 & \mu_1 & 0 & -\delta & 0 \\ 0 & 0 & \mu_2 & 0 & -\delta \end{pmatrix} \quad (2)$$

The eigenvalues of (2) are

$$-\delta, -\delta, -\delta, \frac{\beta_1\Lambda}{\gamma_1\Lambda+\delta} - (\delta+\delta_1+\mu_1), \frac{\beta_2\Lambda}{\gamma_1\Lambda+\delta} - (\delta+\delta_2+\mu_2) \quad (3)$$

We determine the basic reproduction number, $\mathcal{R}_0$, by using the next generation method (Driessche, 2017), i.e.

$$\mathcal{R}_0 = \max(\mathcal{R}_{01}, \mathcal{R}_{02}) \quad (4)$$

where

$$\mathcal{R}_{01} = \frac{\beta_1\Lambda}{(\gamma_1\Lambda+\delta)(\delta+\delta_1+\mu_1)}, \mathcal{R}_{02} = \frac{\beta_2\Lambda}{(\gamma_1\Lambda+\delta)(\delta+\delta_2+\mu_2)}.$$

Equation (3) is rewritten as

$$-\delta, -\delta, -\delta, \mathcal{R}_{01} - 1, \mathcal{R}_{02} - 1 \quad (5)$$

We conclude the following proposition for the stability of disease-free equilibrium.

Proposition 2. (The stability of disease-free equilibrium.) The disease-free equilibrium is $E_0 = \left(\frac{\Lambda}{\delta}, 0,0,0,0\right)$ is a stable node if $\mathcal{R}_0 < 1$ and it is a saddle point if $\mathcal{R}_0 > 1$.

For condition $\mathcal{R}_0 = 1$ will be discuss in section 3.4.

One Variant Exists

Assume $I_2, R_2 \neq 0$. The condition $I_1 = 0$ implies $R_1 = 0$, the dynamic of the System (1) follows the subsystem

$$\begin{aligned} \frac{dS}{dt} &= \Lambda + \lambda R_2 - S\left(\delta + \frac{\beta_2 I_2}{1+\gamma_1 S}\right), \\ \frac{dI_2}{dt} &= \frac{\beta_2 S}{1+\gamma_1 S} - \delta - \delta_2 - \mu_2 + \frac{\alpha_{22}\beta_2 R_2}{1+\gamma_2 R_2}, \\ \frac{dR_2}{dt} &= \mu_2 I_2 - R_2\left(\delta + \frac{\alpha_{22}\beta_2 I_2}{1+\gamma_2 R_2}\right). \end{aligned} \quad (6)$$

DOI:https//doi.org/10.22452/mjs.vol44no2.5
Malaysian Journal of Science 44(2): 52-62 (June 2025)

We get an equilibrium $E_2 = (S_2, 0, I_{22}, 0, R_{22})$ whose the R_{22}-component satisfies:

$$a_3(R_{22})^3 + a_2(R_{22})^2 + a_1 R_{22} + a_0 = 0 \quad (7)$$

where

$$\begin{aligned} k &= \delta + \delta_2 + \mu_2 \\ a_3 &= (\alpha_{22}\beta_2\gamma_1 - \gamma_1\gamma_2 k + \beta_2\gamma_2)(\alpha_{22}\beta_2(\lambda - \delta) + \delta\gamma_2 k - \gamma_2\lambda\mu 2) \\ a_2 &= (\alpha_{22}\beta_2)^2(\Lambda\gamma_1 + \delta) + (\alpha_{22}\beta_2)((2\delta k - \Lambda(k+\mu_2))\gamma_2 - \lambda(k+\mu_2))\gamma_1 + \\ &\quad (\Lambda\beta_2 - \delta(k+\mu_2))\gamma_2 - \beta_2(\delta - \lambda)) + \gamma_2(((\Lambda\gamma_2 + 2\lambda)\gamma_1 + \delta\gamma_2)k - \beta_2(\Lambda\gamma_2 + 2\lambda))\mu_2 - 2k\delta(\gamma_1 k - \beta_2) \\ a_1 &= -\alpha_{22}\beta_2\left(((k+\mu_2)\gamma_1 - \beta_2)\Lambda + \delta(k+\mu_2)\right) + \left(((2\Lambda\gamma_2 + \lambda)\gamma_1 + 2\delta\gamma_2)k - (2\Lambda\gamma_2 + \lambda)\beta_2\right)\mu_2 - k\delta(\gamma_1 k - \beta_2) \\ a_0 &= \mu_2(\Lambda\gamma_1 k + \delta k - \Lambda\beta_2) \end{aligned}$$

and

$$\begin{aligned} S_2 &= \frac{(\delta + \delta_2 + \mu_2)(\gamma_2 R_{22} + 1) - \alpha_{22}\beta_2 R_{22}}{(\gamma_2 R_{22} + 1)(\beta_2 - \gamma_1(\delta + \delta_2 + \mu_2) + \alpha_{22}\beta_2\gamma_1 R_{22})} \\ I_{22} &= \frac{\delta R_{22}(\gamma_2 R_{22} + 1)}{\mu_2 + \mu_2\gamma_2 R_{22} - \alpha_{22}\beta_2 R_{22}} \end{aligned}$$

With a similar analysis, assume $I_1, R_1 \neq 0$. The condition $I_2 = 0$ implies $R_2 = 0$, we get an equlibrium $E_1 = (S_1, I_{11}, 0, R_{11}, 0)$ and the expression for S_1, I_{11}, R_{11} is similar with S_2, I_{22}, R_{22} by replacing $\alpha_{22}, \beta_2, \delta_2, \mu_2$ with $\alpha_{11}, \beta_1, \delta_1, \mu_1$.

Two Variant Exist

The double endemic equilibrium $\bar{E} = (\bar{S}, \bar{I_1}, \bar{I_2}, \bar{R_1}, \bar{R_2})$ exist if

$$\begin{aligned} \Lambda + \lambda(\bar{R_1} + \bar{R_2}) - \bar{S}\left(\delta + \frac{\beta_1\bar{I_1}}{1+\gamma_1\bar{S}} + \frac{\beta_2\bar{I_2}}{1+\gamma_1\bar{S}}\right) &= 0, \\ \frac{\beta_1\bar{S}}{1+\gamma_1\bar{S}} - \delta - \delta_1 - \mu_1 + \frac{\alpha_{11}\beta_1\bar{R_1}}{1+\gamma_2\bar{R_1}} &= 0, \\ \frac{\beta_2\bar{S}}{1+\gamma_1\bar{S}} - \delta - \delta_2 - \mu_2 + \frac{\alpha_{22}\beta_2\bar{R_2}}{1+\gamma_2\bar{R_2}} + \frac{\alpha_{12}\beta_2\bar{R_1}}{1+\gamma_2\bar{R_1}} &= 0, \\ \mu_1\bar{I_1} - \bar{R_1}\left(\delta + \frac{\alpha_{11}\beta_1\bar{I_1}}{1+\gamma_2\bar{R_1}} + \frac{\alpha_{12}\beta_2\bar{I_2}}{1+\gamma_2\bar{R_1}}\right) &= 0, \\ \mu_2\bar{I_2} - \bar{R_2}\left(\delta + \frac{\alpha_{22}\beta_2\bar{I_2}}{1+\gamma_2\bar{R_2}}\right) &= 0. \end{aligned}$$

has a solution for $\bar{S}, \bar{I_1}, \bar{I_2}, \bar{R_1}, \bar{R_2} > 0$ or equivalently with

$$\delta\gamma_1\bar{S^2} + \left(\delta + \beta_1\bar{I_1} + \beta_2\bar{I_2} - \gamma_1(\Lambda + \lambda\bar{R_1} + \lambda\bar{R_2})\right)\bar{S} - (\Lambda + \lambda\bar{R_1} + \lambda\bar{R_2}) = 0 \quad (8)$$

Since $\Lambda + \lambda\bar{R_1} + \lambda\bar{R_2} > 0$, we conclude that only one positive $\bar{S}$ if discriminant of (8) is positive

$$\begin{aligned} &(\lambda\gamma_1)^2\left(\bar{R_1}^2 + \bar{R_2}^2\right) + 2\lambda\gamma_1(\delta + \gamma_1\lambda\bar{R_2} + \Lambda\gamma_1 - \beta_1\bar{I_1} - \beta_2\bar{I_2})\bar{R_1} + 2\lambda\gamma_1(\delta + \Lambda\gamma_1 - \beta_1\bar{I_1} \\ &-\beta_2\bar{I_2})\bar{R_2} + (\Lambda\gamma_1 + \delta)^2 + (\beta_1\bar{I_1} + \beta_2\bar{I_2})^2 + 2\beta_1\bar{I_1}(\delta - \Lambda\gamma_1) + 2\beta_2\bar{I_2}(\delta - \Lambda\gamma_1) > 0 \end{aligned}$$

Bifurcation Analysis

In the following propositions, we analytically demonstrate the conditions that make transcritical or fold bifurcations occur (see Strogatz (2018) for the bifurcation theory).

Proposition 3. (Transcritical bifurcation) At $\mathcal{R}_{0i} = 1$ or equivalently with $\delta_i = \frac{\Lambda\beta_i}{\Lambda\gamma_1 + \delta} - \delta - \mu_i$, the equilibria E_0 and E_i undergo transcritical bifurcation.

Proof 3. It is simple to get that

i) E_0 and E_1 collide when $\delta_1 = \frac{\Lambda\beta_1}{\Lambda\gamma_1 + \delta} - \delta - \mu_1$ or equivelently with $\mathcal{R}_{01} = 1$, and

ii) E_0 and E_2 collide when $\delta_1 = \frac{\Lambda\beta_1}{\Lambda\gamma_1 + \delta} - \delta - \mu_1$ or equivelently with $\mathcal{R}_{02} = 1$.

At the transcritical point, they become degenerate equilibrium with one zero eigenvalue.

DOI:https//doi.org/10.22452/mjs.vol44no2.5
Malaysian Journal of Science 44(2): 52-62 (June 2025)

Proposition 4. (Fold bifurcation of E_i) Let $D := 18a_3a_2a_1a_0 - 4a_3a_1^3 - 4{a_2}^3a_0 + {a_2}^2{a_1}^2 - 27a_3^2a_0^2 = 0$
where

$k = \delta + \delta_i + \mu_i$

$a_3 = (\alpha_{ii}\beta_i\gamma_1 - \gamma_1\gamma_2 k + \beta_i\gamma_2)(\alpha_{ii}\beta_i(\lambda - \delta) + \delta\gamma_2 k - \gamma_2\lambda\mu_i)$

$a_2 = (\alpha_{ii}\beta_i)^2(\Lambda\gamma_1 + \delta) + (\alpha_{ii}\beta_i)((2\delta k - \Lambda(k + \mu_i)\gamma_2 - \lambda(k + \mu_i))\gamma_1 +$
$(\Lambda\beta_i - \delta(k + \mu_i))\gamma_2 - \beta_i(\delta - \lambda)) + \gamma_2(((\Lambda\gamma_2 + 2\lambda)\gamma_1 + \delta\gamma_2)k - \beta_i(\Lambda\gamma_2 + 2\lambda))\mu_i - 2k\delta(\gamma_1 k - \beta_i)$

$a_1 = -\alpha_{ii}\beta_i\left(((k + \mu_2)\gamma_1 - \beta_i)\Lambda + \delta(k + \mu_i)\right) + + \left(((2\Lambda\gamma_2 + \lambda)\gamma_1 + 2\delta\gamma_2)k - (2\Lambda\gamma_2 + \lambda)\beta_i\right)\mu_i - k\delta(\gamma_1 k - \beta_i)$

$a_0 = \mu_i(\Lambda\gamma_1 k + \delta k - \Lambda\beta_i)$

Fold bifurcation of E_i occurs when $D = 0$.

Proof 4. Without loss of generality, we prove the fold bifurcation of E_2. Since R_i is the root of the cubic equation (7), the discriminant of it (10) can be computed using the Cardano formula (Wituła & Słota, 2010). If $D = 0$, then the cubic equation (7) has multiple roots, and all of its roots are real.

4. Numerical Simulation

This section presents the codimension two bifurcation diagram, from which we can show some interesting phase portraits and time series. The initial parameters are given in Table 3. We vary the parameters α_{22} and δ_2 to analyze how the new variant impacts the pandemic situation.

Table 3. The initial parameter set.

α_{11}	α_{12}	α_{22}	β_1	β_2	δ	δ_1	δ_2	Λ	λ	μ_1	μ_2	γ_1	γ_2
0.01	0.35	0.24	0.08	0.5	0.0065	0.04	0.02	0.02	0.0125	0.8	0.7	0.1	0.05

We have the saddle point $e_0 = (3.076923077, 0, 0, 0, 0)$ and the stable node $e_2 = (0.09463959107, 0, 2.520380824, 0, 7.900874864)$. So one variant exists, for the phase portrait (see Figure 4 (Left)).

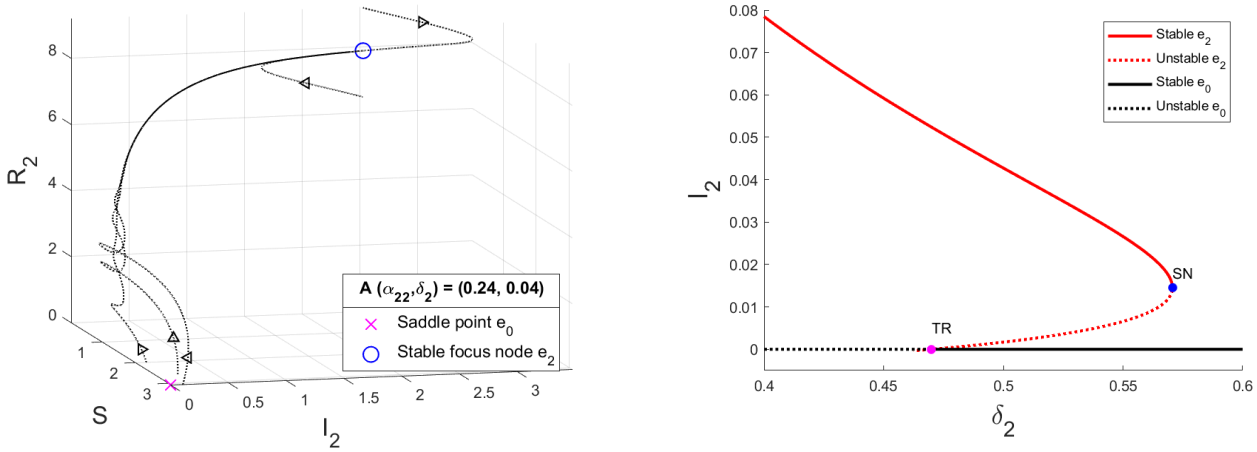

Figure 4. (Left) Some orbits for the initial parameter set in Table 3 or the A parameter set. (Right) The I_2-coordinate of the branch of continuation equilibrium as variation on parameter δ_2.

Codimension One Bifurcation

Using the numerical continuation AUTO, we vary δ_2 and obtain a transcritical bifurcation point (between e_0 and e_2) and a fold (or saddle node) bifurcation point for e_2 (see Table 4). These are the same results with Propositions 3 and 4.

Table 4. Transcritical and fold bifurcations list.

Bifurcation	**Label**	δ_2	S	I_1	I_2	R_1	R_2
Transcritical	TR	0.469970711	3.076923077	0	0	0	0
Fold	SN	0.570633209	2.939313201	0	0.014559724	0	1.251406177

Figure 4 (Right) displays the branch of continuation nontrivial equilibrium (red curve), which undergoes a fold bifurcation and a transcritical bifurcation with disease-free equilibrium (black line) as a variation on parameter δ_2. Their stability alternates from stable (solid style) to unstable (dashed style), and vice versa.

DOI:https//doi.org/10.22452/mjs.vol44no2.5
Malaysian Journal of Science 44(2): 52-62 (June 2025)

Codimension Two Bifurcation

In this section, we add α_{22} (which is the reinfection rate parameter of the new variant) as a new free parameter. We then follow the loci of the fold bifurcation and obtain the fold bifurcation curve. As we increase α_{22}, we find the Bogdanov-Takens bifurcation point

$$BT := (\delta_2, \alpha_{22}) = (0.70518678919, 2.0727176300)$$

which means there is a Hopf bifurcation near that point. After we found one Hopf bifurcation point, we followed its loci and obtained the Hopf bifurcation curve. These results are shown in Figure 5 (Left). We give four examples to illustrate the dynamic for each region in Figures 4 (Left), 5 (Right), and 6.

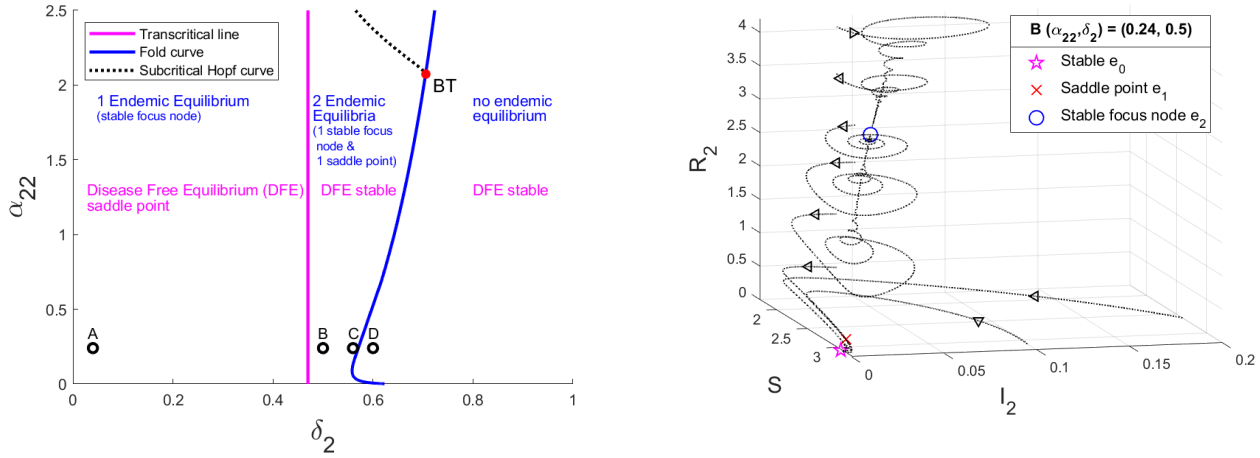

Figure 5. (Left) Two parameter bifurcation diagram of the nontrivial equilibrium of System (1) for $0 \leq \delta_2 \leq 1{,}0 \leq \alpha_{22} \leq 2.5$. (Right) Some orbits for the B parameter set.

The transcritical bifurcation point does not depend on parameter α_{22}, since $\mathcal{R}_0$ does not either, according to formula (4). For $\delta_2 < 0.469970711$, for example, in the A parameter sets in Figure 4 (Left), we have the disease-free equilibria e_0, which is saddle point typed (magenta cross symbol), and the stable focus node e_2 (blue circle symbol). We have two nontrivial equilibriums, e_1 and e_2, but e_1 is negative. By passing through the transcritical line, e_1 becomes positive. Then, e_0 and e_1 switch their stability, so e_0 becomes stable (magenta star symbol), and we obtain the new saddle point e_1 (Figure 5 (Right)). These nontrivials become closer (Figure 6 (Left)), collide and vanish at the fold bifurcation point. As a result, we only have one stable disease-free equilibria e_0, as in Figure 6 (Right).

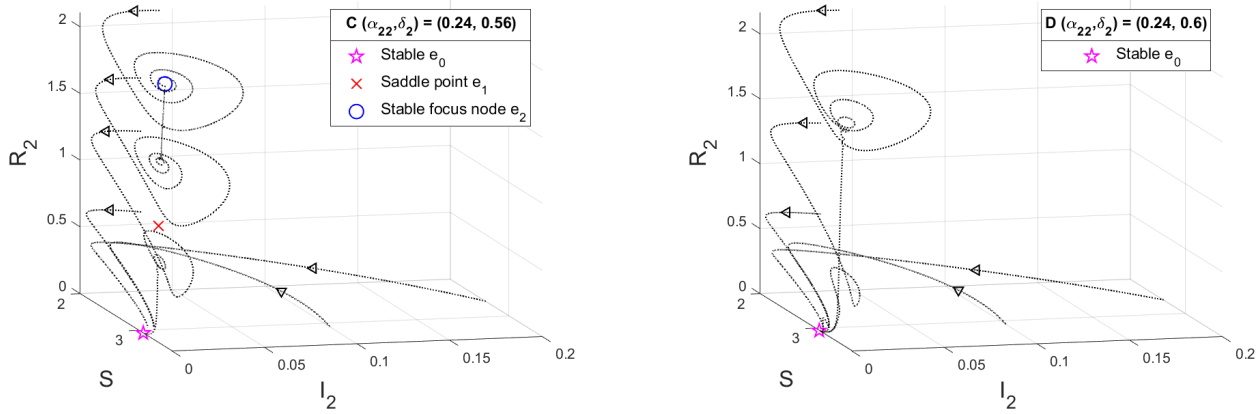

Figure 6. Some orbits for the C and D parameter sets.

We are interested in seeing the dynamics near the Bogdanov-Takens point and focusing on the nontrivial equilibrium e_2. We present four different topological examples to illustrate the dynamics between the C parameter set and the D parameter set (see Figures 8 and 9).

In the previous set of parameters, labeled as the E parameter set and illustrated in Figure 8 (Left), e_2 is a stable focus node (blue circle symbol). However, in the F parameter set, the system undergoes a homoclinic bifurcation. The solution for some initial conditions near the homoclinic orbit (dash-dotted red orbit) will have a very large period (see Figure 8 (Right)).

By increasing δ_2, in the G parameter set, the homoclinic orbit has shrunk and become an unstable limit cycle (dashed blue orbit), as shown in Figure 9 (Left). After passing through the subcritical Hopf curve in the H parameter set, the unstable limit cycle collides with e_2, and e_2 becomes an unstable focus node (blue square symbol), as shown in Figure 9 (Right).

DOI:https//doi.org/10.22452/mjs.vol44no2.5
Malaysian Journal of Science 44(2): 52-62 (June 2025)

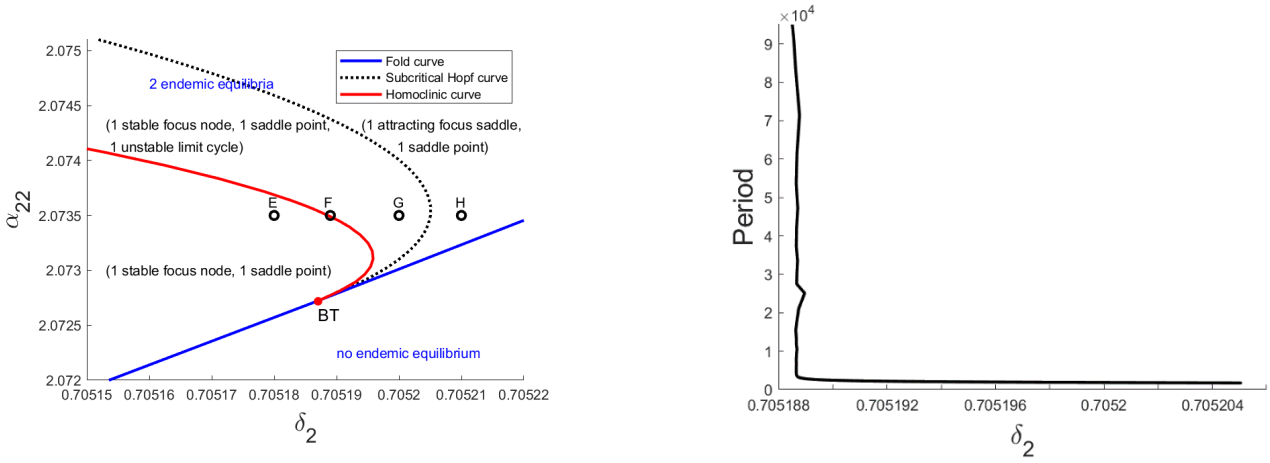

Figure 7. (Left) Two parameter bifurcation diagram of the nontrivial equilibrium of System (1) near the Bogdanov-Takens bifurcation point. (Right) The branch of periodic solution at $\alpha_{22} = 2.0735$ as variation on parameter δ_2. By numerical observation, the homoclinic orbit occurs at $\delta_2 = 0.70518803536$.

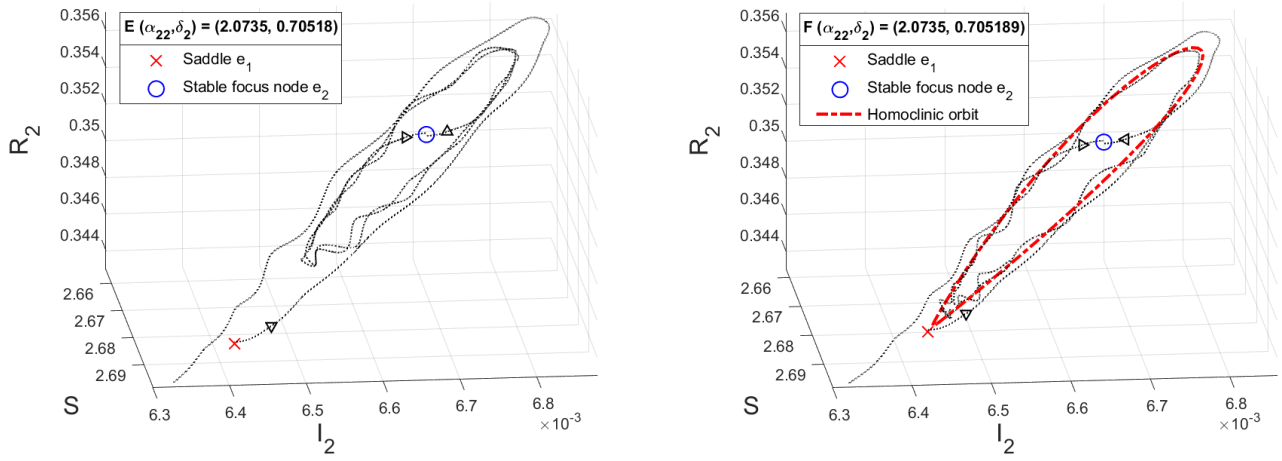

Figure 8. Some orbits for the E dan F parameter set.

5. Conclusion Remarks

We developed a SIRI model to investigate the reinfection rate, α_{22}, and Case Fatality Rate, δ_2, of a new COVID-19 variant in preventing the spread of COVID-19. Our calculations yielded the basic reproduction number $\mathcal{R}_0$, which revealed a stable disease-free equilibrium for all parameter values, provided $\mathcal{R}_0 < 1$. By varying α_{22} and δ_2, we discovered a codimension two bifurcation, known as the Bogdanov-Takens bifurcation. Further numerical analysis allowed us to gain a better understanding of the behavior near this bifurcation point, including the identification of a domain of parameters containing a stable limit cycle and a homoclinic orbit.

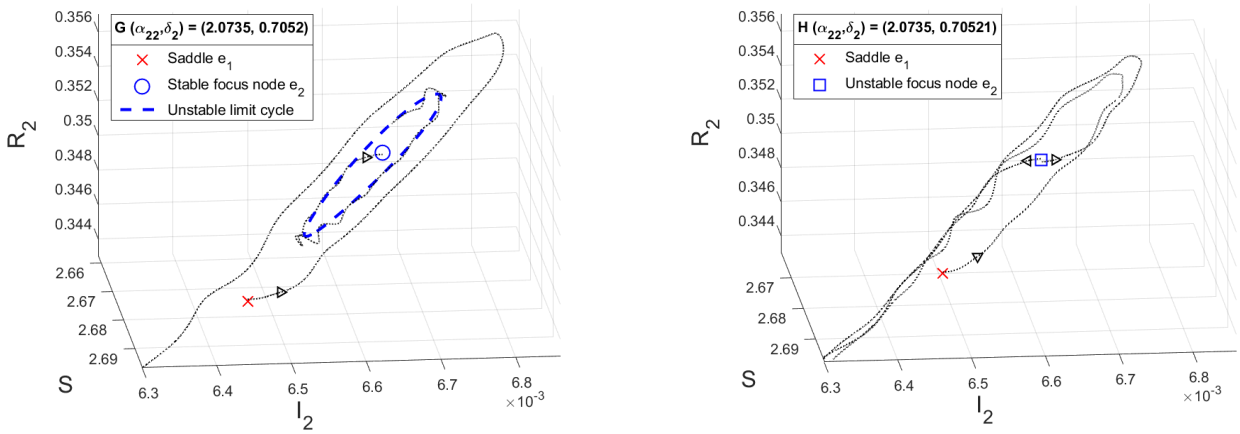

Figure 9. Some orbits for the G and H parameter set.

DOI:https//doi.org/10.22452/mjs.vol44no2.5
Malaysian Journal of Science 44(2): 52-62 (June 2025)

Our simulation of parameter sets A, B, C, E, F, and G demonstrated the persistence of a COVID-19 variation. We examined the manner in which a pandemic could occur based on initial conditions, even with a small infected population, in addition to analyzing infection and mortality rates. We believe that the codimension two bifurcation diagram could provide valuable insight into forecasting the impact of any future COVID-19 variants.

6. Acknowledgement

I would like to acknowledge the Indonesian Mathematical Society (IndoMS) for the research visit grant and give my warmest thanks to Dr. Wirawan Chinviriyasit (King Mongkut's University of Technology Thonburi, Thailand), who made this work possible. I am indebted to Dr. Johan Matheus Tuwankotta for his continuous support and feedback throughout the research process. Furthermore, I also acknowledge the financial support from Lembaga Penelitian dan Pengabdian Masyarakat (LPPM), Parahyangan Catholic University.

7. References

Agusto, F. B. (2013). Optimal isolation control strategies and cost-effectiveness analysis of a two-strain avian influenza model. Biosystems, 113(3), 155-164.

Duan, L., Huang, L., & Huang, C. (2021). Spatial dynamics of a diffusive SIRI model with distinct dispersal rates and heterogeneous environment. Communications on Pure and Applied Analysis, 20(10), 3539-3560.

European Centre for Disease Prevention and Control. Available online: https://www.ecdc.europa.eu/en/infectious-disease-topics/z-disease-list/covid-19/ facts/transmission-covid-19 (accessed on Februari 26, 2024).

Martins, J., & Pinto, A. (2017). Bistability of evolutionary stable vaccination strategies in the reinfection SIRI model. Bulletin of mathematical biology, 79, 853-883.

McMahon, A., & Robb, N. C. (2020). Reinfection with SARS-CoV-2: Discrete SIR (susceptible, infected, recovered) modeling using empirical infection data. JMIR public health and surveillance, 6(4), e21168.

Ndaïrou, F., Area, I., Nieto, J. J., & Torres, D. F. (2020). Mathematical modeling of COVID-19 transmission dynamics with a case study of Wuhan. Chaos, Solitons & Fractals, 135, 109846.

Nurjanah, A., & Prawoto, B. P. (2022). Dinamika Model Siri Covid-19 Dengan Adanya Pengaruh Kerumunan. MATHunesa: Jurnal Ilmiah Matematika, 10(2), 280-288.

Office for National Statistics (ONS) - Coronavirus (COVID-19) Infection Survey in UK. Available online: https://www.ons.gov.uk/peoplepopulationandcommunity/healthandsocialcare/conditionsanddiseases/datasets/coronaviruscovid19infectionsurveydata (accessed on October 19, 2022).

Our World in Data. SARS-CoV-2 sequences by variant. Available online: https://ourworldindata.org/explorers (accessed on May 2, 2023).

Pinto, L. M., Nanda, V., Sunavala, A., & Rodriques, C. (2021). Reinfection in COVID-19: A scoping review. medical journal armed forces india, 77, S257-S263.

Salman, A. M., Ahmed, I., Mohd, M. H., Jamiluddin, M. S., & Dheyab, M. A. (2021). Scenario analysis of COVID-19 transmission dynamics in Malaysia with the possibility of reinfection and limited medical resources scenarios. *Computers in biology and medicine*, *133*, 104372.

Saxena, S. K. (Ed.). (2020). Coronavirus disease 2019 (COVID-19): epidemiology, pathogenesis, diagnosis, and therapeutics. Springer nature.

Sharma, S., Badshah, V. H., & Gupta, V. K. (2017). Analysis of a SIRI Epidemic Model with Modified Nonlinear Incidence Rateand Latent Period. Asian Journal of Mathematics and Statistics, 10, 1-12.

Strogatz, S. H. (2018). Nonlinear dynamics and chaos with student solutions manual: With applications to physics, biology, chemistry, and engineering. CRC press.

Ud Din, R., Shah, K., Ahmad, I., & Abdeljawad, T. (2020). Study of transmission dynamics of novel COVID-19 by using mathematical model. Advances in Difference Equations, 2020, 1-13.

Van den Driessche, P. (2017). Reproduction numbers of infectious disease models. Infectious disease modelling, 2(3), 288-303.

Wangari, I. M., Sewe, S., Kimathi, G., Wainaina, M., Kitetu, V., & Kaluki, W. (2021). Mathematical modelling of COVID-19 transmission in Kenya: a model with reinfection transmission mechanism. *Computational and Mathematical Methods in Medicine*, *2021*, 1-18.

Wituła, R., & Słota, D. (2010). Cardano's formula, square roots, Chebyshev polynomials and radicals. Journal of Mathematical Analysis and Applications, 363(2), 639-647.

Yale Medicine. Will BA.2.86 ('Pirola'), the New Coronavirus Variant, Increase COVID-19 Cases?. Available online: https://www.yalemedicine.org/news/new-covid-variant-ba286-pirola (accessed on September 1, 2023).

DOI:https//doi.org/10.22452/mjs.vol44no2.5
Malaysian Journal of Science 44(2): 52-62 (June 2025)

Yang, Y., Zhou, J., & Hsu, C. H. (2019). Threshold dynamics of a diffusive SIRI model with nonlinear incidence rate. Journal of Mathematical Analysis and Applications, 478(2), 874-896.

Yong, B., Owen, L., & Hoseana, J. (2022). Mathematical Analysis of an Epidemic Model for COVID-19. Letters in Biomathematics, 9(1), 3–22.

Yong, B., Hoseana, J., & Owen, L. (2022). A design of governmental policies for the eradication of COVID-19 in Jakarta using an SIR-type mathematical model. Commun. Math. Biol. Neurosci., 2022 (2022), Article ID 26

World Health Organization (WHO). COVID-19 weekly epidemiological update. Available online: https://www.who.int/publications/m/item/weekly-epidemiological-update-on-covid-19 1-september-2023 (accessed on September 1, 2023).

DOI:https//doi.org/10.22452/mjs.vol44no2.5
Malaysian Journal of Science 44(2): 52-62 (June 2025)